# Welding Residual Stress Characteristics of Bolt-welding Joint in TBM Split Cutterhead

Shuli Zhang[1], Jianfu Zhang[2,*], Zhong Guo[1], Peng Gao[2] and Tianyu Du[2]

[1]School of Mechanical and Electrical Automobile Engineering, Yantai University, Yantai, China

[2]Department of Mechanical Engineering, Tsinghua University, Beijing, China

[*]Corresponding author

***Abstract*—The welding seam of the split cutterhead of tunnel boring(TBM) machine is easy to generate cracks in the working process, which affects the construction process and increases the cost. The double box structure is extracted from TBM cutterhead. The effects of high-strength bolts and welding speeds on the bolt-welding connection were investigated by finite element method. The results show that the area near the weld is subjected to residual tensile stress and the area far from the weld is subjected to residual compressive stress. The distribution of welding residual stress was strongly affected by welding speeds and high-strength bolts.**

***Keywords—TBM split cutterhead; bolt-welding joint; welding residual stress***

## I. INTRODUCTION

The cutterhead of tunnel boring machine(TBM) is huge. To facilitate the processing and transportation, the manufacture of cutterhead is divided into parts fixed by bolt-welding connection. Welding will change the stress state inside the cutterhead, and it is prone to generate cracks and other defects, which have a serious impact on the overall strength. Cracking at the welding is one of the main causes of failure, which affects the construction progress [1-3]. Therefore, it is important to study the welding residual stress characteristics of the split cutterhead joint to improve the fatigue resistance.

In recent years, many scholars carried out a lot of research works on TBM cutterhead. Sun [4-5] studied the failure area of TBM cutterhead, and obtained the split joint is one of the most dangerous areas. Welding defects are the main reason of crack formation. This may result in the cutterhead excessive deformation or failure. Li [6] and Qi [7] found the strong vibration is the main reason of TBM cutterhead short life due to the complex random load of the cutterhead. Zhang [8] and Samuel [9] reported the failure modes of TBM cutterhead and many testing works were done during the cutterhead driving process. Huo [10-11] and Zhu [12] also investigated the effects of welding crack on the fatigue of TBM cutterhead. Wang [13] and Zhang [14] analyzed the energy consumption performance index of the shield machine.

In welding residual stress research, Chen [15-16] compared the numerical simulation heat source models of welding processes. Lu [17] and Nguyen [18] analyzed the simulation technology of the welding. Dong [19] simulated the welding process using different welding sequences, and quantitatively described the influence of welding sequence on welding residual stress and deformation. Teng [20] and Deng [21] developed relevant research on the thermophysical properties of Q345 and its adjacent steel, providing reasonable parameters in the process of welding simulation.

In summary, many works have been done on the investigation of welding residual stresses of TBM cutterhead. However, the bolt-welding residual stress characteristics of the TBM split cutterhead joint are still unclear. This paper focus on the research of bolt-welding residual stress characteristics based on finite element method. A double box structure simulation model is established. The welding temperature and stress fields are calculated by thermo-elastic-plastic theory. Then the effects of bolting on the distribution of welding residual stress are obtained.

## II. STRUCTURAL MODEL

### A. Equivalent Model of the Cutterhead Joint

The TBM cutterhead model was built by Solidworks. The cutterhead model consists of a center block and four side blocks. The tool holders are distributed on the cutterhead. Due to the large size and high manufacturing cost of TBM cutterhead, a double box structure was extracted. It is connected by six 8.8-class M12 high-strength bolts and welding. The structure size is 150×100×150 mm, the plate thickness is 10 mm, and the weld seam is opened at 60° groove, as shown in Figure I. In finite element analysis, the high-strength bolts were simplified and the axial force was equivalent to a surface pressure. The contact pair of the two plates was established by the contact manager module of ANSYS.

FIGURE I. TBM CUTTER HEAD AND DOUBLE BOX STRUCTURE

### B. Welding Process Parameters

The structural material is Q345, and the welding method is $CO_2$ gas shielded welding. During welding process, the changes of material properties are non-linear with the continuous change of temperature. So, reasonable material properties parameters are needed in the simulation calculation, and the parameters are shown in Table I and Table II.

TABLE I. PHYSICAL PARAMETER VALUES OF TEMPERATURE FIELD

| Temperature (℃) | Density (kg/m3) | Specific heat capacity (J/kg.℃) | Heat conduction (W/m.℃) |
|---|---|---|---|
| 25 | 7900 | 470 | 50.7 |
| 100 | 7880 | 490 | 48.2 |
| 300 | 7790 | 550 | 41.5 |
| 500 | 7660 | 645 | 39.2 |
| 700 | 7660 | 860 | 31.8 |
| 900 | 7550 | 680 | 60.0 |
| 1100 | 7410 | 680 | 200 |
| 1300 | 7370 | 650 | 350 |
| 1500 | 7320 | 650 | 500 |

TABLE II. PHYSICAL PARAMETER VALUES OF STRESS FIELD

| Temperature (℃) | Poisson's ratio | Elastic modulus (×e10/Pa) | Linear expansion coefficient (W/m.℃) |
|---|---|---|---|
| 25 | 0.28 | 20.5 | 10.6 |
| 100 | 0.28 | 19.7 | 10.6 |
| 300 | 0.29 | 17.5 | 10.6 |
| 500 | 0.29 | 15.0 | 10.6 |
| 700 | 0.31 | 11.5 | 10.6 |
| 900 | 0.35 | 2.0 | 10.6 |
| 1100 | 0.38 | 0.7 | 10.6 |
| 1300 | 0.38 | 0.5 | 10.6 |
| 1500 | 0.38 | 0.1 | 10.6 |

### *C. Simulation Model*

The double box structure was established through APDL programming and the grid are arranged reasonably. The 8-node hexahedral thermal unit Solid70 was used in temperature field, then the Solid70 was replaced with the structural unit Solid185 to further study the stress field. Figure II shows the finite element model.

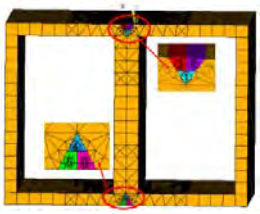

FIGURE II. FINITE ELEMENT MODEL

## III. CHARACTERISTICS OF TEMPERATURE FIELD DISTRIBUTION

The weld filling process is simulated by birth-death element method. All the elements in the weld are active and then deactive when the simulated weld is filled. While the elements are activated, the heat generation rate is applied. The heat generation rate is:

$$HGEN=(K\times U\times I)/(A\times V\times DT) \quad (1)$$

K-welding heat source thermal efficiency, U-welding voltage, I-welding current, A-weld cross-sectional area, V-welding speed, DT-time of each load step. In this paper, K=0.75, U=25 V, I=200 A, A=0.01×0.01×tan(30)/3 m2, DT=0.2 s.

Figure III depicts the temperature distribution of the second weld during filling process. It can be concluded that the welding is a process that changes with time, the material melts when the heat source passes by.

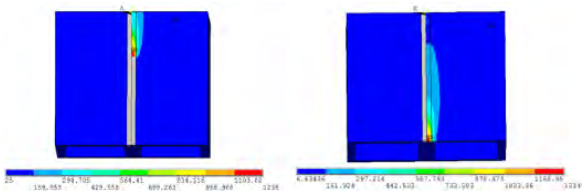

FIGURE III. FILLING PROCESS OF SECOND WELD

Three nodes (n1, n2, n3) are selected to form the PATH1 along the parallel second weld direction, four nodes (n4, n5, n6, n7) are selected to form the PATH2 along the vertical second weld direction, as shown in Figure IV.

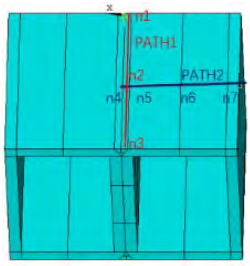


FIGURE IV. PATH1 AND PATH2

### *A. Characteristics of Temperature Field Along Parallel Weld Direction*

Figure V(A) is the temperature-position curve of the second weld at 30 s and 35 s. and When T=30 s, the heat source moves to 100 mm, the temperature reaches the highest. Although there is no heat source in the latter part, the temperature also rises due to the heat transfer. When T=35 s, the heat source moves to 150 mm, the filling is finished. Figure V(B) shows the temperature-time curve of n1, n2 and n3 at 20-40 s. When the heat source passes, the temperature will rise to the melting point of materials. The welding heat source input from n1 and the temperature peak is low. The temperature peak at n2 and n3 increased because of the preheating effect. After the heat source leaves, the welding pool is cooled rapidly.

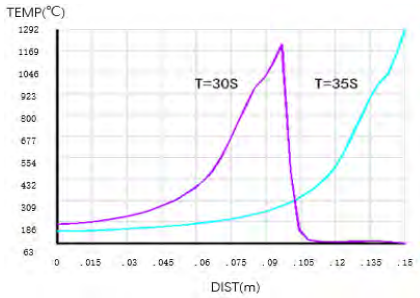


(A) TEMPERATURE-POSITION CURVE OF PATH1

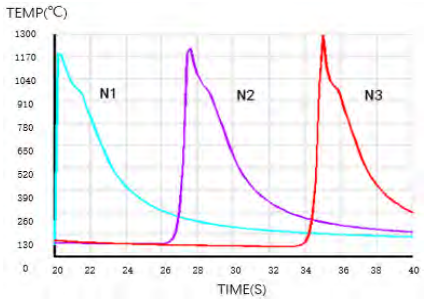


(B) TEMPERATURE-TIME CURVE OF N1- N3

FIGURE V. TEMPERATURE OF PATH1

### B. *Characteristics of Temperature Field Along Vertical Welding Direction*

Figure VI(A) shows the temperature-position curve at 30 s and 35 s. When T=30 s, the heat source is closer to PATH2, so the temperature is higher. When T=35 s, the heat source moves to the end of the welding far away from PATH2, So the temperature is lower. Figure VI(B) shows the temperature-time curve of n4, n5, n6 and n7 at 20-40 s. When the heat source passes through n4, the temperature reaches the melting point of the material in a short time. N5 is close to it, and the temperature rises to about 850 °C. While, the N6 and n7 are far away from the weld, and the heat exchange is not carried out.

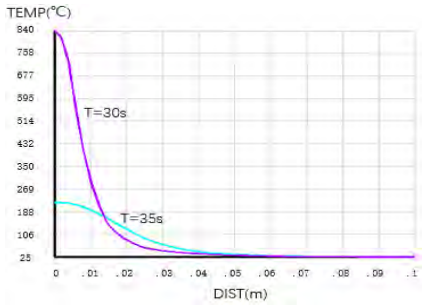


(A) TEMPERATURE-POSITION CURVE OF PATH2

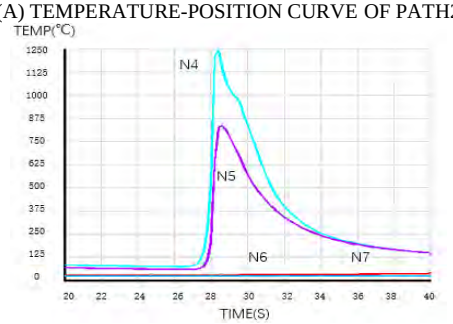


(B) TEMPERATURE-TIME CURVE OF N4- N7

FIGURE VI. TEMPERATURE OF PATH2

## IV. CHARACTERISTICS OF RESIDUAL STRESS

The simulation results of temperature field are applied to the stress field. The corner points of the model are constrained avoiding rigid body displacement and stress release affected by the constraints. The residual stress of welding is analyzed from three aspects: longitudinal residual stress in Z direction, parallel to the axis of the weld; transverse residual stress in X direction, perpendicular to the axis of the weld; transverse residual stress in Y direction, along the thickness of the plate. In the three directions of X, Y and Z, except for the weld, the whole model is in the state of compressive stress, and the tensile stress peak appears at the junction of the two welds, as shown in Figure VII.

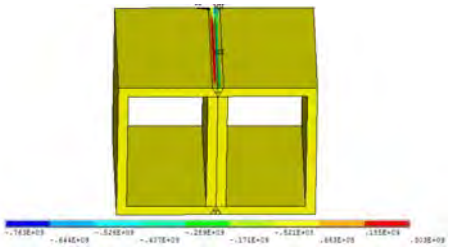

(A) $\sigma_Z$ (Mpa)

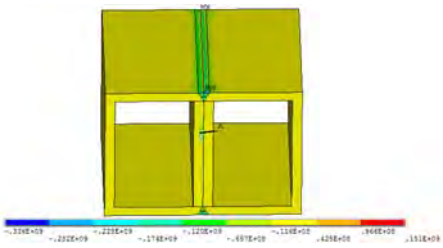

(B) $\sigma_X$ (Mpa)

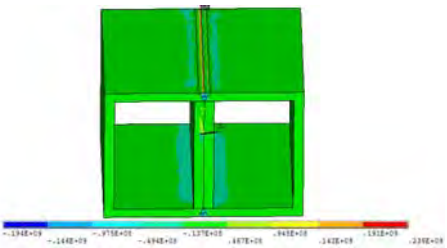

(C) $\sigma_Y$ (Mpa)

FIGURE VII. WELDING RESIDUAL STRESS DISTRIBUTION

### A. *Effects of Welding Speed on Residual Stress*

The welding speeds produces the changes of heat input leading to the change of residual stress distribution. The results are shown in Table III. When the welding speed is small, the stress peak appears in the direction of the plate thickness. However, when the welding speed is large, the stress peak appears in the direction parallel to the weld

TABLE III. STRESS VALUES AT DIFFERENT WELDING SPEEDS

| **Welding speed (mm/s)** | $\sigma_Z$ **(MPa)** | $\sigma_X$ **(MPa)** | $\sigma_Y$ **(MPa)** |
|---|---|---|---|
| 6 | 373 | 234 | 505 |
| 8 | 317 | 127 | 367 |
| 10 | 303 | 151 | 239 |
| 12 | 284 | 155 | 192 |
| 14 | 241 | 138 | 190 |

### B. *Effects of High-Strength Bolts on Residual Stress*

The effects of high-strength bolts on the residual stress characteristics of bolt-welding joint were investigated at different welding speeds. The results are shown in Table IV. The existence of high-strength bolts changes the distribution of welding residual stress: the longitudinal residual stress in Z direction is increasing, the transverse residual stress in X

direction is decreasing, and the transverse residual stress in Y direction is not changed.

TABLE IV. STRESS VALUES OF PURE WELDED/ BOLTED-WELDED STRUCTURES

| Welding speed (mm/s). | Pure welded/ bolted welded $\sigma_Z$ (MPa) | Pure welded/ bolted welded $\sigma_X$ (MPa) | Pure welded/ bolted welded $\sigma_Y$ (MPa) |
|---|---|---|---|
| 8 | 258/317 | 154/127 | 368/367 |
| 10 | 269/303 | 171/151 | 235/239 |
| 12 | 249/284 | 174/155 | 188/192 |

## V. CONCLUSION

The characteristics of temperature field shows that, with the movement of welding heat source, the material near welding seam is melted firstly, and then solidified. The characteristics of stress field results show that the cooled and solidified first welding metal limits the shrinkage of back welding metal. The residual tensile stress of two adjacent welds is large, and the area far from the welding is subjected to residual compressive stress. The characteristics of residual stress are affected by high-strength bolts and welding speeds. So, the high-strength bolts and welding speeds is necessary to be considered during the processing of TBM split cutterhead bolt-welding joint.

## ACKNOWLEDGMENT

The authors gratefully acknowledge the financial support for this research provided by National Natural Science Foundation of China (Grant No. 51575301).

## REFERENCES

[1] Qijun ZHANG, Zhonghai ZHANG, Hong ZHANG, “Discussion on the technology and market demand of shield tunneling machine in China ,” Trenchless technology, 2003, pp. 76-80.

[2] Qihu QIAN, Chaofu LI, Deming FU, “The application status and Prospect of tunnel boring machine in China's underground engineering,” Journal of Underground Space and Engineering, 2002, pp. 1-11.

[3] Mengshu WANG, “Outline of development of Chinese railways, tunnels and underground space,” Tunnel construction, 2010, pp. 351-364.

[4] Wei SUN, Ye ZHU, Jingxiu LING, “Reliability calculation of split cutter head based on crack failure zone,” Journal of Northeast University (Natural Science Edition), 2016, pp. 1144-1148.

[5] Wei SUN, Ye ZHU, Junzhou HUO, “Prediction and analysis of TBM cutter head crack location based on crack failure zone division,” Journal of Mechanical Engineering, 2018, pp. 27-35.

[6] Hongliang LI, “ Cause analysis and repair method of cutter head crack of TB880E Rock Roadheader,” Construction machinery, 2010, pp. 62-67.

[7] Mengxue QI, Yanjun WANG, Hongliang LI, “Research and application of comprehensive renovation technology of open-type roadheader,” Modern tunnel technology, 2009, pp. 64-70.

[8] Z X ZHANG, S Q KOU, X C TAN, “ In-situ measurements of cutter forces on boring machine at Aspo hard rock laboratory,” Rock mechanics and Rock Engineering,2003, pp. 39-61

[9] Samuel S, “Disc force measurements on a full-face tunneling machine,” International Journal of Rock Mechanics and Mining Sciences & Geomechanics Abstracts,1984, pp. 83-96.

[10] Junzhou HUO, Dong ZHU, Guangqi LI, “Application of a small time scale fatigue crack growth model of plane stress/strain transition in life prediction of TBM cutter-head,” Engineering Failure Analysis, 2017, pp. 11-30.

[11] Junzhou HUO, Dong ZHU, Weizheng WANG, “Theoretical crack growth prediction model for thick plate butt welding joints based on stress/strain transitions,” The International Journal of Advanced Manufacturing Technology,2017, pp. 1-16.

[12] Lihui WANG, Yilan KANG, Zongxi CAI, “The energy method to predict disc cutter wear extent for hard rock TBM,” Tunnelling and Underground Space Technology,2012, pp. 183-191

[13] Ling, W Sun, J Huo, L Guo, “Study of TBM cutterhead fatigue crack propagation life based on multi-degree of freedom coupling system dynamics,” Computers & Industrial Engineering,2015, pp. 1-14.

[14] Qian ZHANG, Chuanyong QU, Yilan KANG, “Identification and optimization of energy consumption by shield tunnel machines using a combind mechanical and regression analysis,” Tunnelling and Underground Space Technology,2012, pp. 350-354.

[15] Jiaquan CHEN, “Comparison of heat source models in numerical simulation of welding process,” Welding technology, 2006, pp. 9-11

[16] Jiaquan CHEN, “Advances in numerical simulation of welding process heat source model,” Equipment Manufacturing Technology, 2005, pp. 10-14.

[17] Anli LU, “Some key technical problems and their preliminary studies in the field of welding process simulation.,” China Mechanical Engineering, 2000, pp. 210-214.

[18] Nguyen V N, Nguyen Q M, “Study computational simulation and experimental of Tee-joint by visual-weld software and Tungsten Inert gas welding process,” 2016 International Conference on Advanced Materials for Science and EngineeringTainan,China,2016, pp. 151-154.

[19] Dashan DONG, Xiangdong YU, “Effect of welding sequence on deformation and residual stress of thin-walled box girder.,” Hot working process, 2014, pp. 163-166.

[20] T L TENG, C C LIN, “Effect of welding conditions on residual stress due to butt welds,” International Journal of Pressure Vessels and Piping,1998, pp. 857-864.

[21] D DENG, “FEM prediction of welding distortion and distortion in carbon steel considering phase transformation effects,” Materials and Design, 2009, pp. 359-366.